

Development and *In Vivo* Performance Evaluation of 10-60 MHz Band Impulse-Radio-Based Transceiver for Deep Implantation having 10 Mbps

Jianqing Wang, *Member, IEEE*, Kohei Nomura, Hiroki Narita, Fuminori Ito, Daisuke Anzai, *Member, IEEE*
Jacob Bergsland, and Ilangko Balasingham, *Senior Member, IEEE*

Abstract—In view of the requirements for high-speed, highly reliable wireless implant communication, we have developed an implant transceiver working at 10 - 60 MHz band. The developed transceiver is based on impulse radio technology with multi-pulse position modulation to increase the communication speed and reliability and utilizes the automatic equalization technique to suppress waveform distortion and inter-symbol interference due to frequency-dependent tissue properties. The transmit antenna has a dimension of 2.6 cm × 1.6 cm × 1.6 cm and a relative bandwidth of 16% by forming the radiation elements on a flexible magnetic sheet for miniaturization. Through an *in vivo* experiment on a living swine, we have shown the feasibility of implant communication in a depth up to 26 cm with a minimum data rate of 10 Mbps. These results demonstrate superiority of this new technology over all others reported so far in the literature.

Index Terms—Automatic equalization, implant antenna, implant transceiver, impulse radio, *in vivo* experiment, wireless implant communication.

I. INTRODUCTION

THE aging population is becoming a global social challenge. There is a strong desire to find technological solutions to provide cost-benefit, cost-effective health care services. To this end information and communication technology can play a pivotal role in developing novel applications. For example, various types of *in vivo* biological sensors and *in vivo* medical robots can be used not only to detect biological information and images, but also for long-term function in the abdominal cavity or embedded in organs for continuous diagnosis and treatment. Micro-robots can eventually be expected to move freely within the human body to offer remote treatment or drug injection. To improve bio-sensing and actuator driven techniques, it is essential to establish high-speed and highly reliable wireless implant communication between in- and out-side the human body [1]-[3]. Yuce and Dissanayake summarized the status of implant communications in [4].

Manuscript received xx February, 2018; revised xx xx, 2018, accepted xx xx, 2018. This research and development work was supported in part by the MIC/SCOPE #185006005, Japan, and the Research Council of Norway funded project Wireless In-body Sensors and Actuator Networks (WINNOW) grant no. 270957/O70.

J. Wang, K. Nomura, H. Narita, F. Ito and D. Anzai are with the Graduate School of Engineering, Nagoya Institute of Technology, Nagoya 466-8555, Japan (Corresponding author e-mail: wang@nitech.ac.jp)

J. Bergsland and I. Balasingham are with the Intervention Center, Oslo University Hospital, NO-0027 Oslo, Norway. I. Balasingham also is with the Department of Electronic Systems, Norwegian University of Science and Technology, NO-7491 Trondheim, Norway.

Current implant communications mainly employ the 400 MHz band. Due to the limitation of frequency regulation in this band, a narrow-band modulation scheme must be adopted, which limits the available data rates to several hundred kbps. Since implant communication may be used for *in vivo* image transmission, data rates as high as several Mbps are usually required. To increase the data rate, the authors previously attempted to employ ultra wide band (UWB) technology at its low band (3.4 - 4.8 GHz). However, the transmission experiment in a living swine only demonstrated a possibility to secure a bit error rate (BER) of 10^{-2} at 1 Mbps at a depth of 5 cm [5], which is insufficient for implant applications. Although it was attempted to combine transmit- and receive- diversity to achieve higher data rate [6], no significant improvement on the communication distance was achieved in the body.

The human body is a lossy dielectric medium. The wavelength inside it is shortened due to its frequency-dependent dielectric properties. The dielectric properties are usually expressed using the complex permittivity which is a summation of terms corresponding to various dispersion mechanisms. Four Debye-type dispersion expressions provide good modeling for most human tissues. The corresponding expression of complex permittivity as a function of angle frequency ω is given as [7]

$$\epsilon_r(\omega) = \epsilon_\infty + \sum_{n=1}^4 \frac{\Delta\epsilon_n}{1 + (j\omega\tau_n)^{1-\alpha_n}} + \frac{\sigma_0}{j\omega\epsilon_0} \quad (1)$$

where each term is described in terms of a modified Debye expression. In each dispersion region, $\Delta\epsilon_n$ is the magnitude of dispersion, τ_n is the relaxation time constant, α_n is the deviation from Debye behavior. ϵ_0 is the free-space permittivity, ϵ_∞ is the permittivity when the frequency approaches infinity, and σ_0 is the ionic conductivity. The determined parameters for each tissue are shown in [8]. The frequency-dependent dielectric properties result in severe signal attenuation and waveform distortion when a signal passes through the human body.

Fig. 1 shows a semi-infinite large plane medium of homogeneous human muscle tissue with a normal plane wave incidence to it. The corresponding path loss was calculated theoretically at two typical depth of 5 cm and 10 cm. As compared to 400 MHz band and UWB band, the path loss at 10 - 60 MHz band is much smaller, which can thus provide a significant improvement on the communication distance

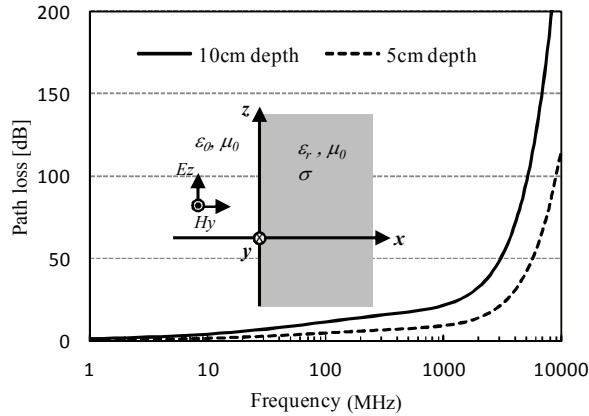


Fig. 1. Frequency dependence of path loss for muscle tissue at depths of 10 cm and 5 cm, respectively for a one-dimensional model.

in the human body. This result suggests that the implant communication is more appropriate at lower frequencies from the point of view of path loss. In addition, the 10 - 60 MHz band falls in the extremely weak radio band in Japan. According to a Japanese radio law, as long as the radiated electric field intensity is lower than $500 \mu\text{V/m}$ at a distance of 3 m, it is legally available for use [9]. This requirement is actually easy to satisfy because of the implant transceiver's small size, low transmit power and usage in lossy media. However, there are two problems that need to be resolved in employing the 10 - 60 MHz band for implant communication. The first is how to raise the data rate up to 10 Mbps or higher, and the other is how to design a wide band implantable antenna with a dimension of 2 - 3 cm.

In this study, we aim to develop the 10 - 60 MHz band implant transceiver to achieve a data rate of up to 10 Mbps at a deep communication distance. To this end, we employ a wide band impulse radio - multi-pulse position modulation (IR-MPPM) scheme, together with an automatic equalizer to suppress the waveform distortion and resultant inter-symbol interference. To realize a small size wide band antenna in this frequency band, we make the transmit signal have a frequency spectrum shape favorable for antenna design, and form the antenna on a material with high magnetic permeability based on the wavelength shortening effect.

This paper is organized as follows. Section II describes the basic implant transmitter structure, signal waveforms and frequency spectra. Section III describes the implant antenna design and their performance evaluation. Section IV describe the receiver structure with automatic equalization, and Section V gives the *in vivo* communication performance evaluation results in a living swine. Section VI concludes this paper.

II. TRANSMITTER STRUCTURE AND PERFORMANCE

Impulse radio (IR) technique has a potential for wide band and high speed communication because it transmits short pulses directly based on digital bits. The feature without carrier signal also contributes to the miniaturization of the implant transmitter. Fig. 2(a) shows the structure of the implant transmitter, and Fig. 2(b) shows its hardware implementation.

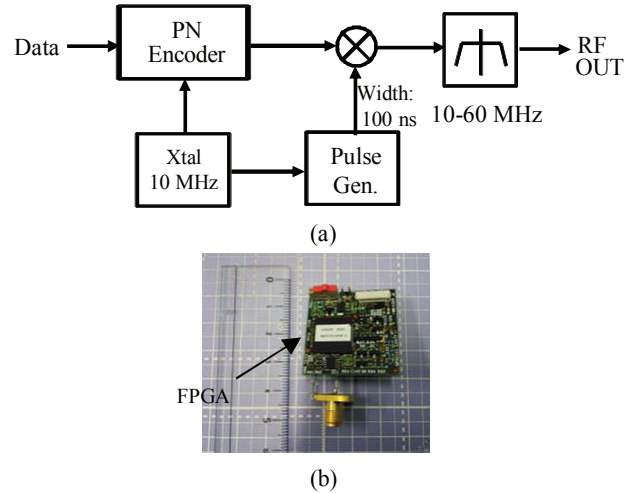


Fig. 2. (a) Structure of the IR-MPPM transmitter. (b) Hardware implementation with FPGA board. The total size is 3 cm \times 3 cm.

The digitized information bit is first encoded with a pseudo noise (PN) code, which is driven by a clock generator at 10 MHz. The PN code may consist of one chip, two chips, four chips or eight chips, determined by the required data rate, and the chip rate is the clock frequency of 10 MHz. If one bit is encoded on one chip, the corresponding data rate is 10 Mbps, while if one bit is encoded on eight chips, the corresponding data rate is 1.25 Mbps. The pulse generator produces the pulse to be transmitted with a width nearly 100 ns. When the chip is "1", the pulse is sent to the band pass filter (BPF), while when the chip is "0", nothing is sent. This looks like an on-off keying (OOK) scheme. However, since multiple chips are used to represent one information bit, for example, as shown in Fig. 3, "10100110" are used to represent information bit "0" and "01011001" are used to represent information "1", the combination of PN encoder and OOK modulation can be considered as an MPPM scheme with $M = 8$. By adjusting the chip number within one-bit period, the data rate can change from 1.25 Mbps ($M = 8$) to 10 Mbps ($M = 1$). The pulse sequences modulated in such a form are then spectrum-formed between 10 - 60 MHz by the BPF at the transmitter output. The transmitter was packaged on a 3 cm \times 3 cm printed circuit board. Except for the crystal oscillator and the BPF, all the other parts such as the PN encoder, pulse generator and multiplier were implemented in a commercially available field programmable gate array (Xilinx, Spartan-6). With the current integrated circuit technology, it is not difficult to integrate all the parts in one chip with a smaller size for actual implant applications.

Fig. 4 shows the time waveform and signal spectrum at the transmitter output measured by a digital oscilloscope (Sampling frequency: 8 GHz; Bandwidth: 1.5 GHz) and a spectrum analyzer, respectively. As can be seen, the pulses have a width of nearly 100 ns, and they are sent out directly according to the PN encoder and OOK modulator. It should be emphasized that, as can be seen from the frequency spectrum, instead of making the signal components cover the entire

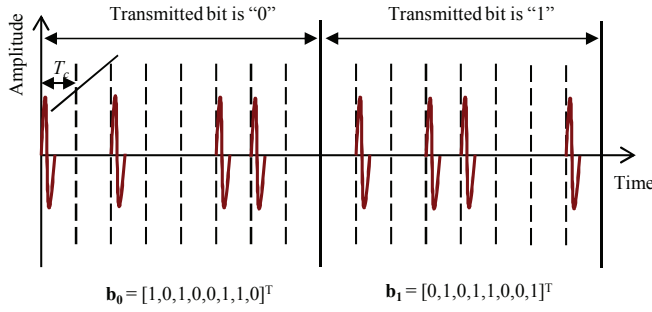


Fig. 3. Concept of the IR-MPPM with $M = 8$.

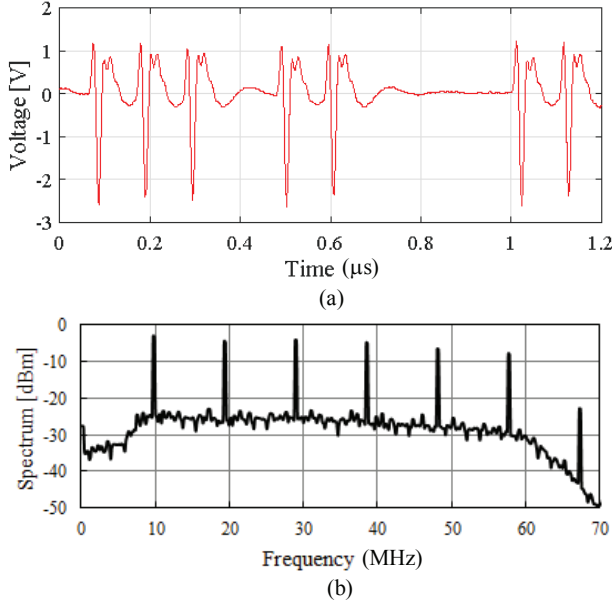


Fig. 4. Example of the transmitted signal. (a) Time waveform. (b) Frequency spectrum.

10 - 60 MHz band, we employed a pulse where the signal components were concentrated at six specific frequencies of 10 MHz, 20 MHz, 29 MHz, 39 MHz, 48 MHz and 58 MHz. This spectrum shape was based on the consideration that it is difficult to design an antenna with a bandwidth as wide as 50 MHz with respect to the central frequency of 35 MHz (relative bandwidth of 1.4). By concentrating the signal components at the six specific frequencies, the implant antenna needs not cover the entire 10 - 60 MHz band. It can be designed to have a narrow bandwidth focusing on these specific frequencies. This greatly ease the difficulty in designing a wide band antenna at this frequency band.

III. ANTENNA STRUCTURE AND PERFORMANCE

The transmit antenna needs to be of small size (2 - 3 cm) for implant application. However, the wavelength λ_0 at 10 - 60 MHz band is around 10 meters in free space. It is essential to shorten the equivalent wavelength for antenna miniaturization. We thus utilized the wavelength shortening effect of material's permeability and permittivity. A magnetic

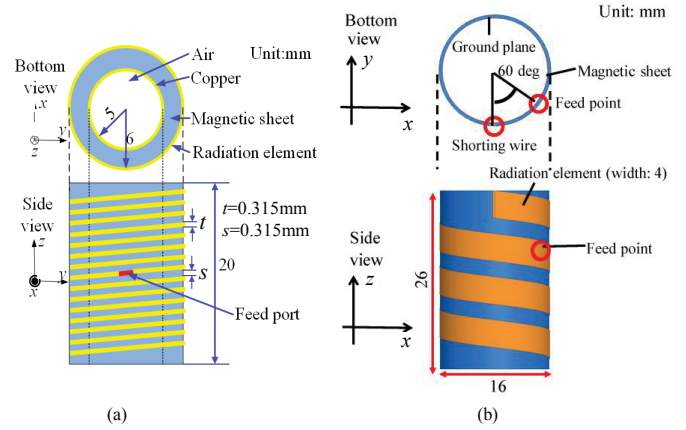


Fig. 5. Designed implant antenna structure. (a) Helical dipole structure. (b) Helical invert-F dipole structure.

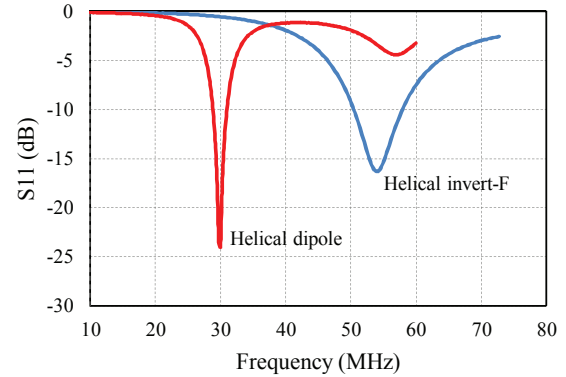


Fig. 6. Measured S_{11} characteristics versus frequency for the two antennas.

material may have both a high relative permeability μ_r and a high relative permittivity ϵ_r . Since the equivalent wavelength $\lambda \cong \lambda_0 / \sqrt{\epsilon_r \mu_r}$, we can expect a double shortening effect by fabricating the antenna radiation element on a magnetic sheet. The flexibility of the magnetic sheet is also beneficial to form a cylindrical shape into which the transmitter circuit can be placed.

Fig. 5 shows two structures of implant antenna design based on the above consideration by using an electromagnetic field simulation tool of finite element method (Ansys, HFSS). The antenna in Fig. 5(a) is a helical dipole structure with a reflection plane [10]. It has a hollow cylindrical shape and consists of three layers. In the first layer, a copper foil with a thickness of 0.1 mm forms the hollow cylinder with a radius of 5 mm, and this acts as the reflection plane of the antenna radiating elements. The second layer is a flexible magnetic sheet with a thickness of 1 mm. The flexible magnetic sheet is a commercially available one with $\mu_r = 20.7$, $\tan\delta_\mu = 0.12$, $\epsilon_r = 13.0$, $\tan\delta_\epsilon = 0.17$, where $\tan\delta_\mu$ is the magnetic loss tangent and $\tan\delta_\epsilon$ is the dielectric loss tangent. The third layer consists of the two dipole elements: two copper wires with a thickness of 0.315 mm. At the two sides of the feeding point, the two wires are wrapped seven turns, respectively, with a

spacing of 0.315 mm.

On the other hand, the antenna in Fig. 5(b) is a helical invert-F dipole structure. It also has a hollow cylindrical shape and consists of three layers. In the first layer, a copper foil with a thickness of 0.1 mm forms the hollow cylinder with a radius of 7.3 mm, and this plays the role of antenna ground. The second layer is the flexible magnetic sheet with a thickness of 0.5 mm, and the third layer is the radiating element formed of a copper foil with a thickness of 0.1 mm and a width of 4 mm. In order to adjust the antenna input impedance, the inverted-F antenna structure is used so that the feeding source between the radiating element and the ground is set at the upside of the cylinder and a short pin between the radiating element and the ground is set at the top of the cylinder.

The two antennas were inserted respectively into a biological-equivalent liquid phantom with a dimension of 28 cm × 16 cm × 28 cm for S_{11} measurement with a network analyzer. The liquid phantom was made of deionized water, sugar, sodium chloride and so on, and its dielectric properties were adjusted to be $\epsilon_r = 56.05$ and conductivity $\sigma = 0.52$ S/m at 30 MHz, nearly 2/3 times muscle's values. The antennas were wrapped in vinyl for insulation from the liquid phantom. Fig. 6 shows measured S_{11} characteristics versus frequency for the two antennas. As can be seen, the helical dipole antenna showed an absolute -10 dB bandwidth of about 2.2 MHz around 30 MHz (relative bandwidth of 7.3%), which can only effectively transmit the signal components around 29 MHz for the spectrum shape in Fig. 4(b). However, the helical invert-F dipole antenna showed an absolute -10 dB bandwidth of about 8.4 MHz (relative bandwidth of 16%). As a result, the signal components at both 48 MHz and 58 MHz can be effectively transmitted. This suggests that the helical invert-F dipole antenna with a dimension of 2.6 cm × 1.6 cm × 1.6 cm may provides a better communication performance than the helical dipole antenna.

IV. RECEIVER STRUCTURE AND PERFORMANCE

The received signal is filtered and amplified, and is then adjusted to an adequate level by a gain controller. Since the signal is in a wide band, the waveform is distorted when passing through the human body due to its frequency-dependent dielectric properties. The band-limited implant antenna is also one of reasons of waveform distortion. So an inter-symbol interference is inevitable in the implant communication. In order to suppress the waveform distortion and inter-symbol interference, implementation of an automatic waveform equalizer to the receiver is desired. Fig. 7(a) shows the receiver structure, and Fig. 7(b) shows its hardware implementation. The automatic equalizer, IR-MPPM demodulator and data storage are implemented in an FPGA (Xilinx, Virtex-6) board with a total size of 26 cm × 10 cm. The analog signal is first analog-digital (AD) converted, and is then input to an automatic equalizer. As a usual equalization method, there are a minimum mean square error (MMSE) method and a zero-forcing (ZF) method. The MMSE method minimizes the mean square error between the transmitted signal and the received signal. Since the amount of calculation is large, it

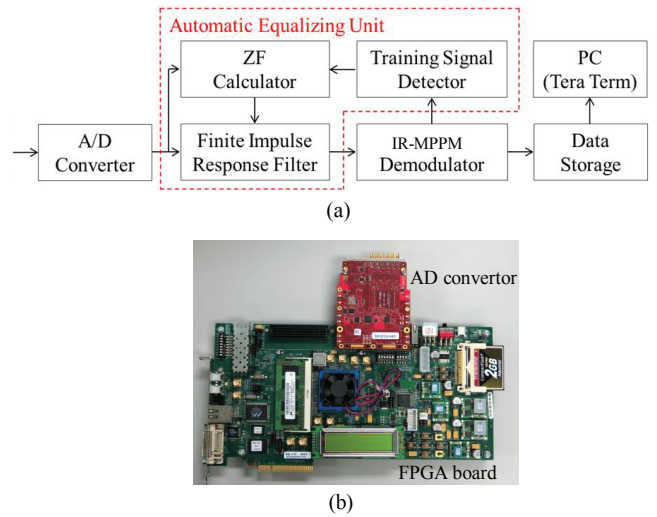


Fig. 7. (a) Structure of the receiver with automatic equalizer. (b) Hardware implementation. The automatic equalizer, IR-MPPM demodulator and data storage are implemented in the FPGA board. The total size is 26 cm × 10 cm.

consumes more power than the ZF method. In contrast, the ZF method forces the receiver output to be zero at all the sampling instances, except for the time instant which corresponds to the transmitted signal. This is easier to be implemented by hardware, and we therefore adopted the ZF method in our receiver.

The ZF method is accomplished by a digital finite impulse response (FIR) filter [11]. When input to the FIR filter is the discrete impulse response h_k of implant communication channel, the output y_k can be expressed as a discrete convolution of the input h_k and the filter coefficient c_n :

$$y_k = \sum_{n=-N}^{n=N} c_n \cdot h_{k-n} \quad (2)$$

where k is the sample number of the discretely sampled time signal, and n is the filter tap number. The ZF method requires $y_k = 0$ for $k \neq 0$ and $y_k = 1$ for $k = 0$. Substitution this condition into (2) yields a set of $2N + 1$ simultaneous equations:

$$\begin{bmatrix} 0 \\ \vdots \\ 1 \\ \vdots \\ 0 \end{bmatrix} = \begin{bmatrix} h_0 & h_{-1} & \cdots & h_{-2N} \\ \vdots & \vdots & & \vdots \\ h_N & h_{N-1} & \cdots & h_{-N} \\ \vdots & \vdots & & \vdots \\ h_{2N} & h_{2N-1} & \cdots & h_0 \end{bmatrix} \begin{bmatrix} c_{-N} \\ \vdots \\ c_0 \\ \vdots \\ c_N \end{bmatrix} \quad (3)$$

To derive the impulse response h_k , the transmitter periodically transmits a known signal sequence as the training signal for the equalizer. The training signal is a random “1” and “0” sequence of 4096 bits arranged between the start bits and the stop bits. By detecting the known sequence in the receiver and storing it in a memory, the transmitted and received training signals are recorded. Then the equalizer calculates the frequency spectrum $R_x(f)$ of the transmitted training signal and $T_x(f)$ of the received training signal by using the fast

TABLE I
IR TRANSCEIVER SPECIFICATIONS

Pulse width	100 ns
Pulse number per bit	8, 4, 2, 1
Frequency band	10 - 60 MHz
Modulation	IR-MPPM
Data rate	1.25, 2.5, 5, 10 Mbps
Maximum output	~ 0 dBm
Demodulation	Envelope detection
Equalization method	ZF method

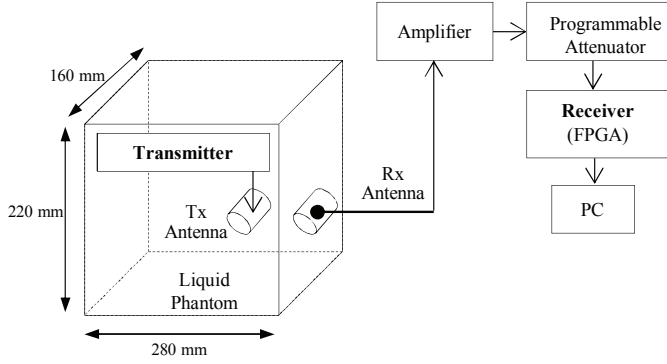


Fig. 8. Experimental setup in a biological-equivalent liquid phantom.

Fourier transform (FFT), and derive the transfer function $H(f)$ from $R_x(f)/T_x(f)$. In such a way, we can derive the impulse response h_k by applying the inverse fast Fourier transform to the transfer function $H(f)$, and obtain the filter coefficient c_n by solving the set of (3) with the derived channel impulse response. So the influence of the communication path can be canceled by the FIR filter from the received signal. Since the coefficients of the digital FIR filter are periodically updated, the receiver adapts to the channel characteristics in real time. After the automatic equalizer, the envelope of equalized signal is extracted and is judged as chip “0” or “1” by a comparator. Then they are further decoded to reproduce the transmitted information bits.

Table I summarizes the specifications of the developed transmitter and receiver. Both the transmitter and the receiver

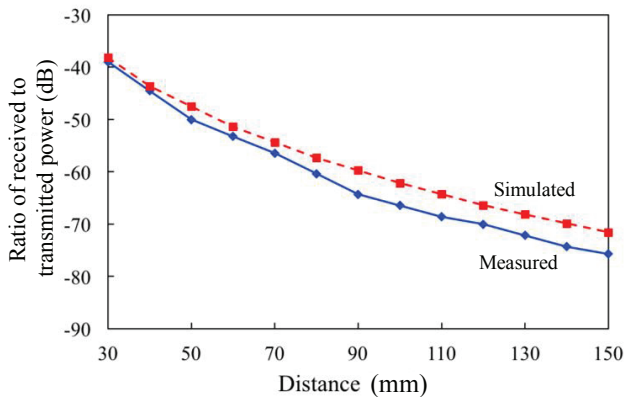


Fig. 9. Comparison between simulated and measured ratios of the power received in the FPGA-implemented receiver to the power transmitted from the FPGA-implemented transmitter for the helical invert-F antenna.

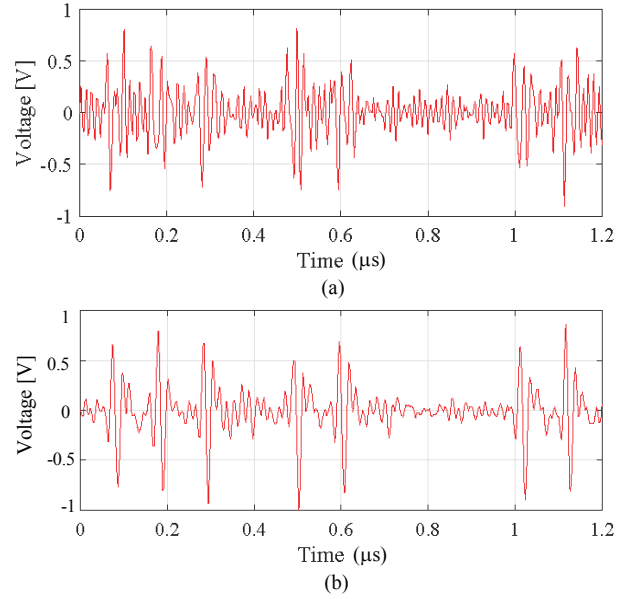


Fig. 10. Comparison of time waveforms of received signals. (a) Without equalization. (b) With equalization.

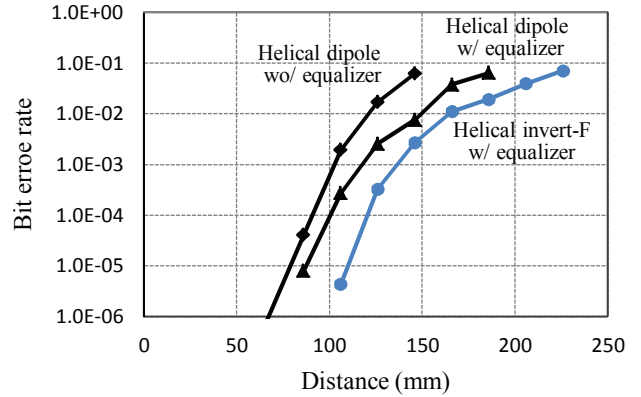


Fig. 11. Comparison of measured BERs for implant communication in the liquid phantom.

were implemented in a FPGA board. The FPGA’s design language is Verilog-HDL which consists of a simulator to examine whether the designed transmitter and receiver codes work. After the debug in the simulator for an assumed received signal, the designed codes were written into the FPGA boards, and the FPGA boards worked as the transmitter and receiver, respectively. It should be noted that, since the maximum transmit power is around 0 dBm (1 mW), the localized ten-gram averaged specific absorption rate (SAR) will be much smaller than the general safety limit of 2 W/kg [12] even if we consider a worst case where the transmit power is completely absorbed in ten grams of human tissue. Fig. 8 shows the setup of experimental validation in a biological-equivalent liquid phantom as described in Section III. The transmitter together with either the helical dipole antenna or the helical invert-F antenna was wrapped with vinyl and inserted in the liquid phantom. The receiver together with the same type

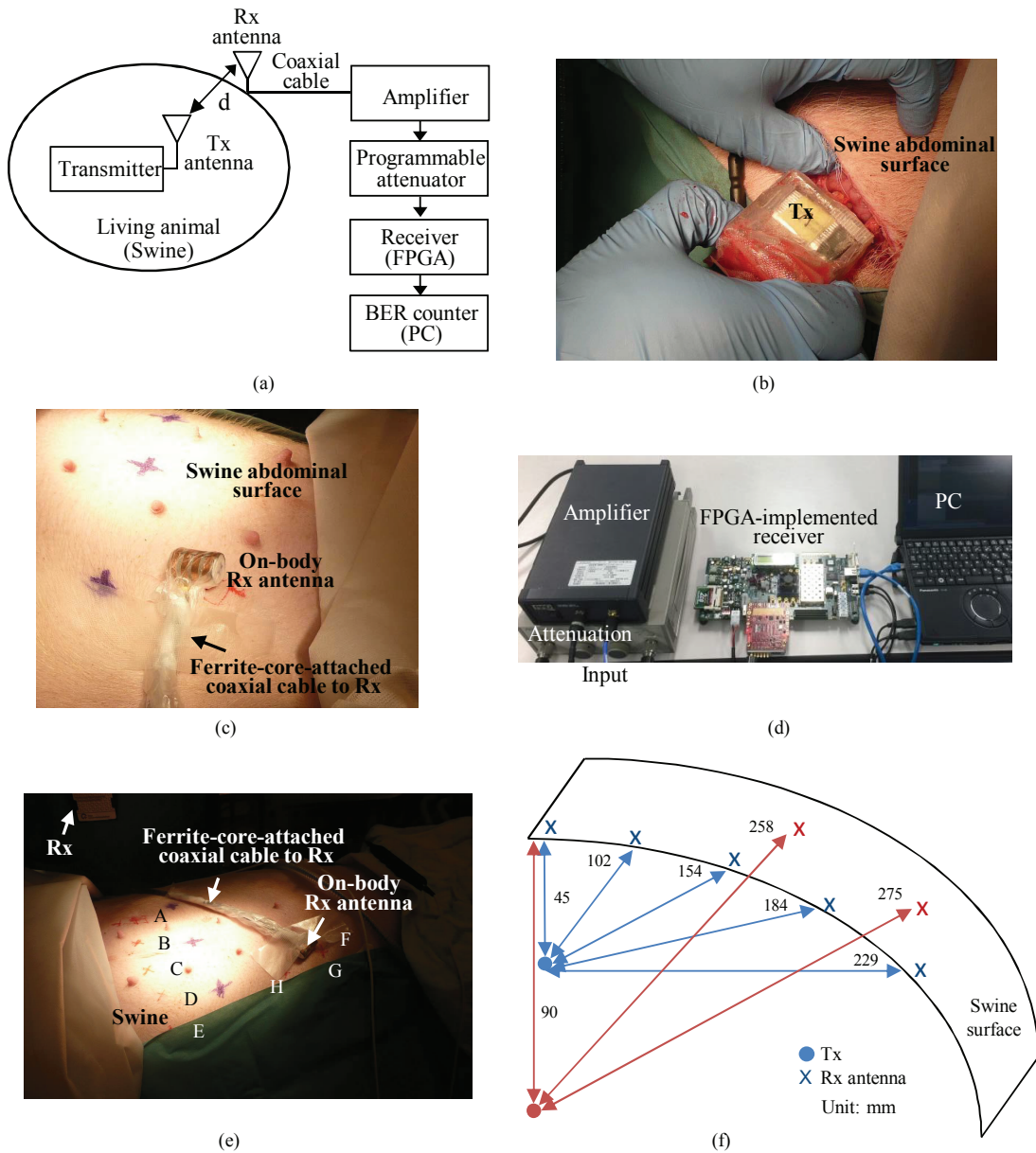


Fig. 12. *In vivo* experiment of implant communication. (a) Block diagram of the *in vivo* experiment with a living swine. (b) View of the implant transmitter to be inserted into the swine’s abdomen. (c) View of a helical invert-F antenna for receiver on the swine’s abdominal surface. (d) The receiver consisting of an amplifier, a programmable attenuator and an FPGA board. (e) View of the *in vivo* experiment consisting of the arrangement of the swine, the on-body receive antenna and the receiver. The marks from A to G on the swine’s abdominal surface denote the receive antenna positions. (f) Positions of the implant transmitter and corresponding communication distances to the on-body receive antenna.

antenna was set on the phantom surface with a spacing of 5 mm, and connected to a personal computer via USB interface for recording the received data and counting the BER. First, instead of a direct comparison of BERs between the FPGA simulator and the phantom experiment, we made a comparison between simulated and measured ratios of the power received in the FPGA-implemented receiver to the power transmitted from the FPGA-implemented transmitter. Fig. 9 shows the results for the helical invert-F antenna. Although there are some deviations between the FPGA simulator and experimental results as the communication distance increases, they are generally in agreement.

Then, to confirm the equalization effect, we measured the signal waveform before and after the equalizer at the receiver. Fig. 10 compares the input signals to the IR-MPPM demodulator with and without the equalizer. It is evident that, by comparing them with Fig. 4(a), the designed equalizer improves the signal quality and mitigates the inter-symbol interference. The correlation coefficient with respect to the transmit signal was improved from 0.4 to 0.7 at a communication distance of 10 cm.

Fig. 11 shows the measured BER performance as a function of distance from the implant transmitter to the receive antenna on the phantom surface at a data rate of 10 Mbps. As can be

seen, the BER performance with the automatic equalizer was totally improved by nearly one digit and the communication distance is significantly extended compared to before. The best BER performance was obtained when the helical invert-F antenna was used. As a result, with the automatic equalizer, we accomplished a BER smaller than 10^{-2} , an acceptable BER level in the physical layer, at a communication distance of up to 16 cm for the data rate as high as 10 Mbps.

V. *In Vivo* EXPERIMENT ON A LIVING SWINE

After the validation experiment of the biological-equivalent liquid phantom, we carried out an *in vivo* implant communication experiment on a living swine. The approval of the Norwegian Animal Research Authority was acquired before we carried out the living animal experiment at the Oslo University Hospital, Norway. During the experiment, we provided humane treatment to the animal in accordance to standard clinical protocol defined in Article 23 of EU Directive 2010/63.

Fig. 12 shows the *in vivo* experiment setup of implant communication. Fig. 12(a) is the block diagram of the *in vivo* experiment. Fig. 12(b) shows the implant transmitter to be inserted into the swine's abdomen, and Fig. 12(c) shows a helical invert-F antenna for receiver on the swine's abdominal surface. Fig. 12(d) shows the receiver consisting of a low noise amplifier, a programmable attenuator, and an FPGA board. Fig. 12(e) is an overview of the *in vivo* experiment consisting of the arrangement of the swine, the on-body receive antenna and the receiver. The marks from A to G on the swine's abdominal surface denote the receive antenna positions. The abdomen of the swine was first laparotomized, and the developed implant transmitter together with the helical invert-F antenna, covered with vinyl for insulation, were inserted inside it at a depth of 4.5 cm and 9 cm, respectively. Then the cut wound of the abdomen of swine was stitched for realizing an implant communication situation. The same type receive antenna on the swine's abdomen surface was connected to the receiver by a ferrite-core-attached coaxial cable, and the receiver was connected to a personal computer via USB interface for BER count. The communication distances between the implant transmitter and the on-body receive antenna were measured using an electromagnetic tracking system (NDI, Aurora). After the implant transmitter position and the on-body receive antenna position were fixed, we first measured the distance between them using the electromagnetic tracking system, and then started the implant communication and BER measurement. The communication distances thus obtained are shown in Fig. 12 (f). The main tissue types between the transmitter and the receive antenna were small intestine, fat, muscle and skin.

Fig. 13 shows measured BER performances versus communication distance in the swine with and without the equalizer. The BER performance was improved by the equalizer at all communication distances. A BER smaller than 10^{-2} was accomplished up to 26 cm at 10 Mbps. This result is somewhat better than that in the liquid phantom, and should be attributed to that the liquid phantom simulated tissue properties closer to muscle, yielding a path loss larger than what was seen

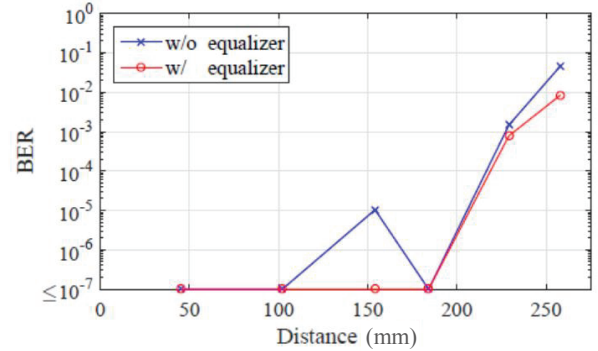


Fig. 13. Measured BERs versus communication distance at 10 Mbps.

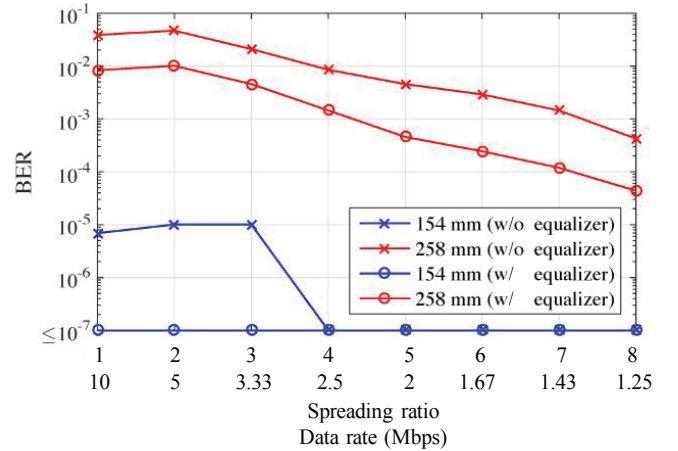


Fig. 14. Measured BERs for different data rates at various communication distances.

in the swine's abdomen. Also, a BER degradation at 15 cm was observed in Fig. 13. This is because that different communication routes consist of different tissue types and thickness. High water-content tissue such as small intestine has larger path loss, whereas low water-content tissue such as fat has smaller path loss. The implant communication performance is therefore dependent on not only the communication distance but also on the tissue types and thickness between the transmitter and receiver. By using the automatic equalizer, this BER degradation was improved obviously.

Moreover, we evaluated the BER performance when multiple pulses were used to represent one bit for further improving the communication performance instead of sacrificing the data rate. The BER performances were obtained for various spreading ratios, in other words, different data rates. In this case, each information bit was encoded by a PN sequence with a spreading ratio from 1 to 8, that corresponded to data rates from 10 Mbps to 1.25 Mbps. Fig. 14 shows the BER performance as a function of spreading ratio from 1 to 8. As can be seen, the BER was obviously improved with the increase of spreading ratio or the decrease of data rate. For example, at the communication distance of 25.8 cm, the BER was improved from 10^{-2} to 10^{-3} by changing the spreading ratio from 1 to 4 (the data rate from 10 Mbps to 2.5 Mbps) in

the case with equalizer. From Fig. 14, the BER can be secured below 10^{-2} up to a communication distance of 26 cm at a data rate of 2.5 Mbps in the case without equalizer and 10 Mbps in the case with equalizer. These *in vivo* experimental results demonstrated a highest data rate, which has been reported so far, in a communication distance as deep as 26 cm in a living body.

VI. CONCLUSIONS

There is a strong desire to develop high-speed, high-reliable wireless implant communication technology for various medical and health care applications. For this purpose we have studied and developed an implant transceiver working at 10 - 60 MHz band with the employment of the impulse radio technology using multi-pulse position modulation scheme. By using an automatic equalizer with the zero forcing method to suppress the waveform distortion and inter-symbol interference due to frequency-dependent tissue properties, the correlation coefficient between the received signal and the transmitted signal has been improved from 0.4 to 0.7. By forming the antenna radiation elements on a flexible magnetic sheet to shorten the equivalent wavelength for antenna miniaturization, the implant antenna has been produced with a dimension of $2.6 \text{ cm} \times 1.6 \text{ cm} \times 1.6 \text{ cm}$ and a relative bandwidth of 16%. Through the *in vivo* experiment on a living swine, we have achieved an implant communication performance with a bit error rate smaller than 10^{-2} and a data rate as high as 10 Mbps at a depth of up to 26 cm. The proposed implant transceiver has the best results reported so far in the literature in terms of transmitter power, data rate and depth.

The future objective is to integrate the implant transceiver circuits into one module for practical use and verification.

REFERENCES

- [1] *IEEE Standard for Local and Metropolitan Area Networks - Part 15.6: Wireless Body Area Networks*, IEEE Standard 802.15.6-2012, Feb. 2012.
- [2] J. Wang and Q. Wang, *Body Area Communications*, Wiley-IEEE, 2012.
- [3] E. Monton, *et al.*, "Body area network for wireless patient monitoring," *IET Commun.*, vol. 2, no. 2, pp. 215-222, Feb. 2008.
- [4] M. R. Yuce and T. Dissanayake, "Easy-to-swallow wireless telemetry," *IEEE Microw. Mag.*, vol. 13, no. 6, pp. 90-101, Sep. 2012.
- [5] D. Anzai, K. Katsu, R. Chavez-Santiago, Q. Wang, D. Plettemeier, J. Wang, and I. Balasingham, "Experimental evaluation of implant UWB-IR transmission with living animal for body area networks," *IEEE Trans. Microw. Theory Techn.*, vol. 62, no. 1, pp. 183-192, Jan. 2014.
- [6] Y. Shimizu, D. Anzai, R. Chavez-Santiago, P. A. Floor, I. Balasingham, and J. Wang, "Performance evaluation of an ultra wideband transmit diversity in a living animal experiment," *IEEE Trans. on Microw. Theory Techn.*, vol.65, no.7, pp.2596-2606, July 2017.
- [7] S. Gabriel, R. W. Lau, and C. Gabriel, "The dielectric properties of biological tissues: III. Parametric models for the dielectric spectrum of tissues", *Phys. Med. Biol.*, vol. 41, no. 11, pp. 2271-2293, Nov. 1996.
- [8] C. Gabriel, "Compilation of the dielectric properties of body tissues at RF and microwave frequencies," *Brooks Air Force Technical Report*, AL/OE-TR-1996-0037, 1996.
- [9] The Radio Use Website, Online Available: <http://www.tele.soumu.go.jp/j/ref/material/rule/> (in Japanese), 2015.
- [10] J. Wang, J. Liu, K. Suguri and D. Anzai, "An in-body impulse radio transceiver with implant antenna miniaturization at 30 MHz," *IEEE Microw. Compon. Lett.*, vol.25, no.7, pp.484-486, July 2015.
- [11] S. Haykin, *Adaptive Filter Theory*, 2nd ed., Prentice Hall, 1996, pp.217-220.
- [12] *IEEE Standard for Safety Levels with Respect to Human Exposure to Radio Frequency Electromagnetic Fields, 3 kHz to 300 GHz*, IEEE Std C95.1-2005, Oct. 2005.



Jianqing Wang (M'99) received the B.E. degree in electronic engineering from the Beijing Institute of Technology, Beijing, China, in 1984, and the M.E. and D.E. degrees in electrical and communication engineering from Tohoku University, Sendai, Japan, in 1988 and 1991, respectively.

He was a Research Associate with Tohoku University and a Senior Engineer with Sophia Systems Co., Ltd., prior to joining the Nagoya Institute of Technology, Nagoya, Japan, in 1997, where he has been a Professor since 2005. His research interests include biomedical communications and electromagnetic compatibility. He authored the book "Body Area Communications" (Wiley-IEEE) in 2012.



Kohei Nomura received the B.E. and M.E. degrees in electrical and electronic engineering from the Nagoya Institute of Technology, Nagoya, Japan, in 2016 and 2018, respectively.

As a Graduate Student at the Nagoya Institute of Technology, he was involved in the study of implant communications. He is currently with Mitsubishi Electric Corporation, Japan.



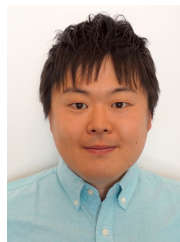
Hiroki Narita received the B.E. and M.E. degrees in electrical and electronic engineering from the Nagoya Institute of Technology, Nagoya, Japan, in 2014 and 2016, respectively.

As a Graduate Student at the Nagoya Institute of Technology, he was involved in the study of implant communications. He is currently with Aisin Seiki Co. Ltd., Aichi, Japan.



Fuminori Ito received the B.E. and M.E. degrees in electrical and electronic engineering from the Nagoya Institute of Technology, Nagoya, Japan, in 2015 and 2017, respectively.

As a Graduate Student at the Nagoya Institute of Technology, he was involved in the study of implant antennas. He is currently with DENSO TECHNO Co. Ltd., Aichi, Japan.



Daisuke Anzai (S'06-A'11-M'14) received the B.E., M.E. and Ph.D. degrees from Osaka City University, Osaka, Japan in 2006, 2008 and 2011, respectively.

Since 2011, he has been with the Graduate School of Engineering, Nagoya Institute of Technology, Nagoya, Japan, as an Assistant Professor, and where he is currently an Associate Professor. He received many awards, including the 2015 IEEE MTT-S Japan Young Engineer Award and the Telecommunications Technology Award from the Telecommunications Advancement Foundation. He has engaged in the research of biomedical communication systems and localization systems in wireless communication networks.



Jacob Bergsland received his medical degree in 1973, and Ph.D. degree in 2011, respectively, from Oslo University, Norway.

After Internship in Norway he moved to the US for education in surgery. He became a specialist in general surgery in 1981, cardiothoracic surgery in 1983. He was Director of Cardiac Surgery at Buffalo VA Hospital, Director of Cardiac Transplantation Program at Buffalo General Hospital, Director of Center for Less Invasive Cardiac Surgery, Clinical Associate Professor of Surgery State University of New York at Buffalo. He was also Initiator of Hospital Partnership between Buffalo General Hospital and Tuzla Medical Center, Bosnia, in 1995, Developer of cardiovascular surgery and cardiology in Bosnia and Herzegovina. He is currently a Researcher and Co-Investigator at The Intervention Centre, Oslo University Hospital, Medical Director at BH Heart Centre, Tuzla BIH, and Medical Director at Medical Device Company, Cardiomech AS. Dr. Bergsland has been Project Leaders of numerous humanitarian and scientific grants, and has 148 peer reviewed publications.



Ilango Balasingham (S'91-M'98-SM'11) received the M.Sc. and Ph.D. degrees from the Department of Electronics and Telecommunications, Norwegian University of Science and Technology (NTNU), Trondheim in 1993 and 1998, respectively, both in signal processing. He performed his Master's degree thesis at the Department of Electrical and Computer Engineering, University of California Santa Barbara, USA.

From 1998 to 2002, he worked as Research Engineer developing image and video streaming solutions for mobile handheld devices at Fast Search & Transfer ASA, Oslo, which is now part of Microsoft Inc. Since 2002 he has been with the Intervention Center, Oslo University Hospital, where he heads the Section for Medical ICT R&D. He was appointed as Professor of Medical Signal Processing and Communications at NTNU in 2006. For the academic year 2016/2017 he was Professor by courtesy at the Frontier Research Institute, Nagoya Institute of Technology in Japan. His research interests include super robust short range communications for both in-body and on-body sensors, body area sensor network, microwave short range sensing of vital signs, short range localization and tracking mobile sensors, and nanoscale communication networks. He has authored or co-authored over 225 journal and conference papers, 7 book chapters, 42 abstracts, 6 patents, and 20 articles in popular press, and has given 16 invited/ keynotes at the international conferences. In addition he is active in organizing conferences (Steering Committee Member of ACM NANOCOM 2018-2021; General Chair: the 2019 IEEE Int. Symposium of Medical ICT, the 2012 Body Area Networks (BODYNETS) conference; TPC Chair of the 2015 ACM NANOCOM) and editorial board (Area Editor of Elsevier Nano Communication Networks 2013-until now).